Received: 8 September 2021 | Revised: 30 October 2021 | Accepted: 13 November 2021

IET Nanobiotechnology

DOI: 10.1049/nbt2.12074

The Institution of Engineering and Technology WILEY

ORIGINAL RESEARCH

Fabrication of superparamagnetic adsorbent based on layered double hydroxide as effective nanoadsorbent for removal of Sb (III) from water samples

Rokhsareh Motallebi | **Ali Moghimi** | **Hamidreza Shahbazi** | **Hakim Faraji**

Department of Chemistry, Islamic Azad University, Varamin, Iran

Correspondence

Rokhsareh Motallebi, Department of Chemistry, Islamic Azad University, Varamin-Pishva Branch, Varamin, Iran.
Email: alimoghimi@iauvaramin.ac.ir and kamran9537@yahoo.com

Funding information

Islamic Azad University

Abstract

In this study, the superparamagnetic adsorbent as Fe@Mg-Al LDH was synthesised by different methods with two steps for the removal of heavy metal ions from water samples. An easy, practical, economical, and replicable method was introduced to remove water contaminants, including heavy ions from aquatic environments. Moreover, the structure of superparamagnetic adsorbent was investigated by various methods including Fourier transform infrared spectroscopy, field emission scanning electron microscopy, energy-dispersive X-ray spectroscopy, and vibrating sample magnetometer. For better separation, ethylenediaminetetraacetic acid ligand was used, forming a complex with antimony ions to create suitable conditions for the removal of these ions. Cadmium and antimony ions were studied by floatation in aqueous environments with this superparamagnetic adsorbent owing to effective factors such as pH, amount of superparamagnetic adsorbent, contact time, sample temperature, volume, and ligand concentration. The model of Freundlich, Langmuir, and Temkin isotherms was studied to qualitatively evaluate the adsorption of antimony ions by the superparamagnetic adsorbent. The value of loaded antimony metal ions with Fe@Mg-Al LDH was resulted at 160.15 mg/g. The standard deviation value in this procedure was found at 7.92%. The desorption volume of antimony metal ions by the adsorbent was found to be 25 ml. The thermodynamic parameters as well as the effect of interfering ions were investigated by graphite furnace atomic absorption spectrometry.

KEYWORDS

graphite furnace atomic absorption, heavy metal ions, layered double hydroxide, replicable method

1 | INTRODUCTION

Organic pollutants are biodegradable, whereas metal ions are non-biodegradable. Hence, metal ions should be removed from wastewaters before discharging it to the environment [1]. Following the growing population and industrialisation of human life, extensive environmental problems have been created by carcinogenic compounds due to the presence of heavy metals. Therefore, many studies have been conducted to remove compounds from water, air, and soil. The layered double hydroxide (LDH) is one of the most popular adsorbents that has received a lot of attention today due to its ease of preparation, affordability, environmental friendliness, and non-toxicity [2–6]. LDH has recently gained the attention of chemists in the use of these materials as organic and inorganic composites. LDHs have relatively weak intra-layer bonds and thus have a high ability to capture organic and inorganic ions. LDHs have numerous applications, for example, catalysts in chemical reactions, photocatalysts, anion exchangers, sensors, plastic additives, removal of heavy metals from the soil, and wastewater heavy-metal precipitating agents. The general formula for LDHs is shown as $[M^{II}_{1-x} M^{III}_{x} (OH)_2](A)^{x+}_{x/m}\cdot nH_2O$. Generally, M^{2+} is a divalent cation such as Ni^{2+}, Fe^{2+}, Co^{2+}, Mg^{2+} etc., and M^{3+} is a trivalent cation such as Fe^{3+}, Al^{3+}, Cr^{3+}, and so on. The value of x in the formula for LDHs is usually chosen to be around 0.20–0.33, which is proportional to the mole fraction $M^{3+}/(M^{2+} + M^{3+})$. A represents an interlayer anion with a

capacity of m such as NO_3^-, CO_3^{2-}, Cl^- and SO_4^{2-}. The values of M^{2+}, M^{3+}, x, and A^m can vary over a wide range [7–11]. Wataru et al. used YVO_4: Eu^{3+} nanoparticles that have a negative surface charge because citrate anions are adsorbed on their surface. The negative charge of YVO_4: Eu^{3+} nanoparticles and the positive charge of LDH nanoplates are placed on the layers of quartz glass with the layer-by-layer (LbL) method to create multilayer films that are held together by electrostatic forces. The researchers found a relationship between the number of deposition cycles and the intensity of photoluminescence of multilayer films [12].

In general, centrifugation and filtration methods are used to separate the adsorbent material from aqueous solution [13]. These applications are time consuming and require extra cost [14]. Compared with traditional centrifugation and filtration methods, magnetic separation method is an efficient, fast and economic method for the separation of magnetic adsorbents from the medium after the adsorption treatment of pollutants is completed [15]. The separation of non-magnetic adsorbents from sample solution after adsorption process is very difficult and also time consuming. This problem can be solved by the incorporation of magnetic nanoparticles on the surfaces of nanocomposite adsorbents and then by using a magnet [16]. Fe_3O_4 nanoparticles are the most widely used materials in the preparation of magnetic nanocomposite adsorbents owing to their unique properties such as chemical stability, uniform particle size, and biocompatibility [17].

One of the most important applications of superparamagnetic nanoparticles is solid-phase extraction (SPE). In this method, superparamagnetic nanoparticles are used as a solid phase. Superparamagnetic nanoparticles can have many potential applications in ferrofluids, colour imaging, magnetic refrigeration, detoxification of biological fluids, synthesis of organic matter as a catalyst, degradative separation, controlled delivery of anticancer drugs, and magnetic cell separation. Due to their special properties, magnetic nanoparticles can be used as adsorbents in the separation, extraction, and removal of various organic and inorganic compounds, especially environmental pollutants, and separation of drugs from biological samples. These features include easy synthesis of nanoparticles, high surface area to volume due to nanometre dimensions, superparamagnetic properties that cause these particles to respond to the external magnetic field and lose their magnetic properties in the absence of an external field, the ability to easily and quickly extract different species using only an external magnetic field, no need for filtration, centrifugation during the extraction process, the ability to extract from large volumes of samples, and the ability to modify the surface of nanoparticles that enable selectivity [18–23].

Ethylenediaminetetraacetic acid is known by the acronym EDTA. It is an amino polycarboxylic acid with the appearance of a water-soluble crystalline white powder and the chemical formula $C_{10}H_{16}N_2O_8$. EDTA is known to be a widely used chelating agent in industrial and domestic purposes and can be used in a variety of fields such as agriculture, medicine, and electroplating. For example, EDTA is used in lead poisoning at a rate of 1 g every 12 h as an intravenous injection. It significantly reduces the amount of lead in the body. Regardless of the charge of other metal ions, EDTA combines with them in a ratio of 1: 1. This reaction is important not only because of the formation of the chelate with all the cations but also because most of these chelates are so stable that they have laid the foundation for volumetric methods. There is no doubt that this high stability is due to the presence of several complexing sites within the molecule, which leads to a cage-like structure, enclosing the cation and keeping it out of the reach of solvent molecules. EDTA is very effective due to its low biodegradability in the groundwater system. EDTA has six potential sites to bond with metal ions, including 4 carboxyl groups and two amine groups [24, 25].

Atomic absorption spectroscopy (AAS) is an excellent multi-purpose method in analytical chemistry. The concentration of toxic trace elements in well water and several other common elements such as calcium, sodium, as well as very small amounts of other metals can be measured by this method. The concentration of rare toxic elements in drinking water and some other common elements such as calcium, sodium, as well as very small concentrations of other metals can be measured by this method. Other applications include measuring lead or cadmium in a drop of blood, measuring silver in synthetic rainwater, searching for impurities in alloys, activating reagents, water analysis, direct analysis of air, direct analysis of metal ores and refined metals, and measuring alloying elements in steel such as manganese, magnesium, chromium, copper, nickel, molybdenum, vanadium, cobalt, titanium, tin, aluminium and lead [26, 27].

In aquatic environments, antimony is found in two forms, Sb (III) and Sb (V), both of which are toxic. However, Sb (III) is 10 times more toxic than Sb (V). Sb (III) is mostly found in groundwater and Sb (V), in surface water [28, 29]. A person comes in contact with antimony by breathing in antimony dust, drinking water, and eating the foods that contain it. It also enters the body through skin contact with soil, water, and materials that are soaked in it. It is dangerous to inhale antimony combined with oxygen in the gas phase. Prolonged contact with this metal at doses above 9 mg/m^3 through air can cause eye, skin, and lung irritation. More serious problems, such as lung disease, heart problems, diarrhoea, vomiting, and stomach ulcers, can occur if contact continues. However, it is not entirely clear whether this element causes infertility or cancer. At a controlled dose, this element is suitable for the treatment of parasitic infections, but it causes health problems at higher doses [30].

This study was conducted with the aim of investigating the removal of antimony ions from aqueous environments modified by these magnetic nanoparticles with EDTA ligands. The conditions for achieving the goal were created, which were optimised taking into account the effective factors. The quality of adsorption, reversibility, and irreversibility was also assessed.

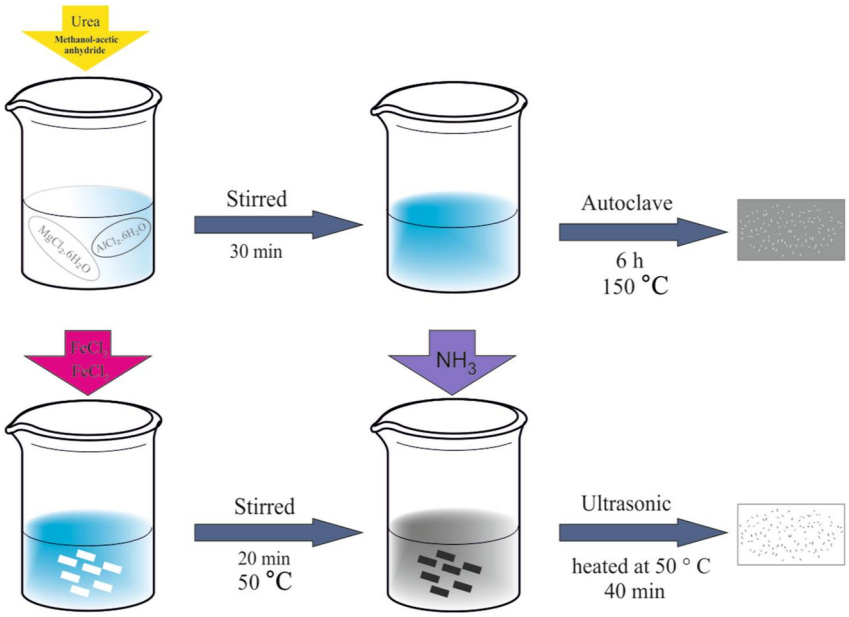

FIGURE 1 The synthesis scheme of Fe@Mg-Al layered double hydroxide

2 | EXPERIMENTAL

Aluminium chloride hexahydrate ($AlCl_3{\cdot}6H_2O$), Iron (II) chloride ($FeCl_2$), Ferric chloride ($FeCl_3$), ethylenediaminetetraacetic acid (EDTA), and potassium antimony (III) oxide tartrate trihydrate ($C_8H_4K_2O_{12}Sb_2{\cdot}H_2O$) were obtained from Sigma-Aldrich. Magnesium chloride hexahydrate ($MgCl_2{\cdot}6H_2O$), methanol-acetic anhydride, and ammonia were obtained from Merck.

2.1 | Equipment

The PG990 Atomic Absorption Spectrometer was used to evaluate the amount of antimony adsorption on the synthesised adsorbent. The A1.8 Tesla magnet was used to separate the magnetic nanoadsorbent from the samples during the optimisation process. An autoclave, a vacuum oven, and an ultrasonic probe were also used to synthesise magnetic adsorbents. During the optimisation process, the incubator shaker with the refrigerator was used to adjust the temperature. The formation of functional groups was demonstrated using the PerkinElmer (spectrum two model) FTIR test. The TESCAN MIRA3 FESEM made in Czechoslovakia and energy dispersive X-ray spectroscopy (EDS) analysis equipped with IDFix software were used to study the surface morphology of synthesised magnetic nanoparticles. In addition, the crystal structure of the sample was determined using the X-ray diffraction (XRD) test performed by the X'pertpro device from Panalytical. The saturation magnetisation of the synthesised magnetic nanoparticles was measured using a vibrating sample magnetometer (VSM) test with LBKFB (Meghnatis Daghigh Kavir Co.). The surface zeta potential of the adsorbent was studied using a zeta potential apparatus (SZ100, Horiba Co.).

2.2 | Synthesis method for Fe@Mg-Al LDH

To fabricate the superparamagnetic nanoadsorbent, which is done in two phases, initially, 48.7 g of $MgCl_2{\cdot}6H_2O$, 2.96 g of $AlCl_2{\cdot}6H_2O$, 5.09 g of urea, and 12 ml of methanol-acetic anhydride were stirred on a magnetic stirrer for 30 min. When the solution became clear, it was placed in an autoclave for 6 h at 150°C. The solid phase was then separated from the liquid using a centrifuge and washed with water and ethanol. The white product was then dried at 120°C for 12 h. In the next step, 0.12 g of the white product obtained from the previous step was added to 0.08 g of $FeCl_2$,·0.216 g of $FeCl_3$, and 20 ml of deionised water. Afterwards, the container containing the sample was placed on a magnetic stirrer at 50°C for 20 min. After cooling the solution of a black sample, it was homogenised by an ultrasonic device, and then 1 ml of ammonia solution was added at the same time, and it was placed on a heater at 50°C after 40 min. Finally, the black product was washed with distilled water, was separated from the liquid by a magnet, and dried at room temperature (Figure 1).

2.3 | Adsorption parameters studies

The amount of adsorption efficiency in each phase of the optimisation was obtained from Equations (1) and (2):

$$R(\%) = \frac{c_0 - c_e}{c_0} \times 100 \quad (1)$$

$$q_e = \frac{c_0 - c_e}{M} \times V \quad (2)$$

where C_0 is the initial concentration of a metal ion in the sample solution (mg L^{-1}), C_e is the metal ion concentration in

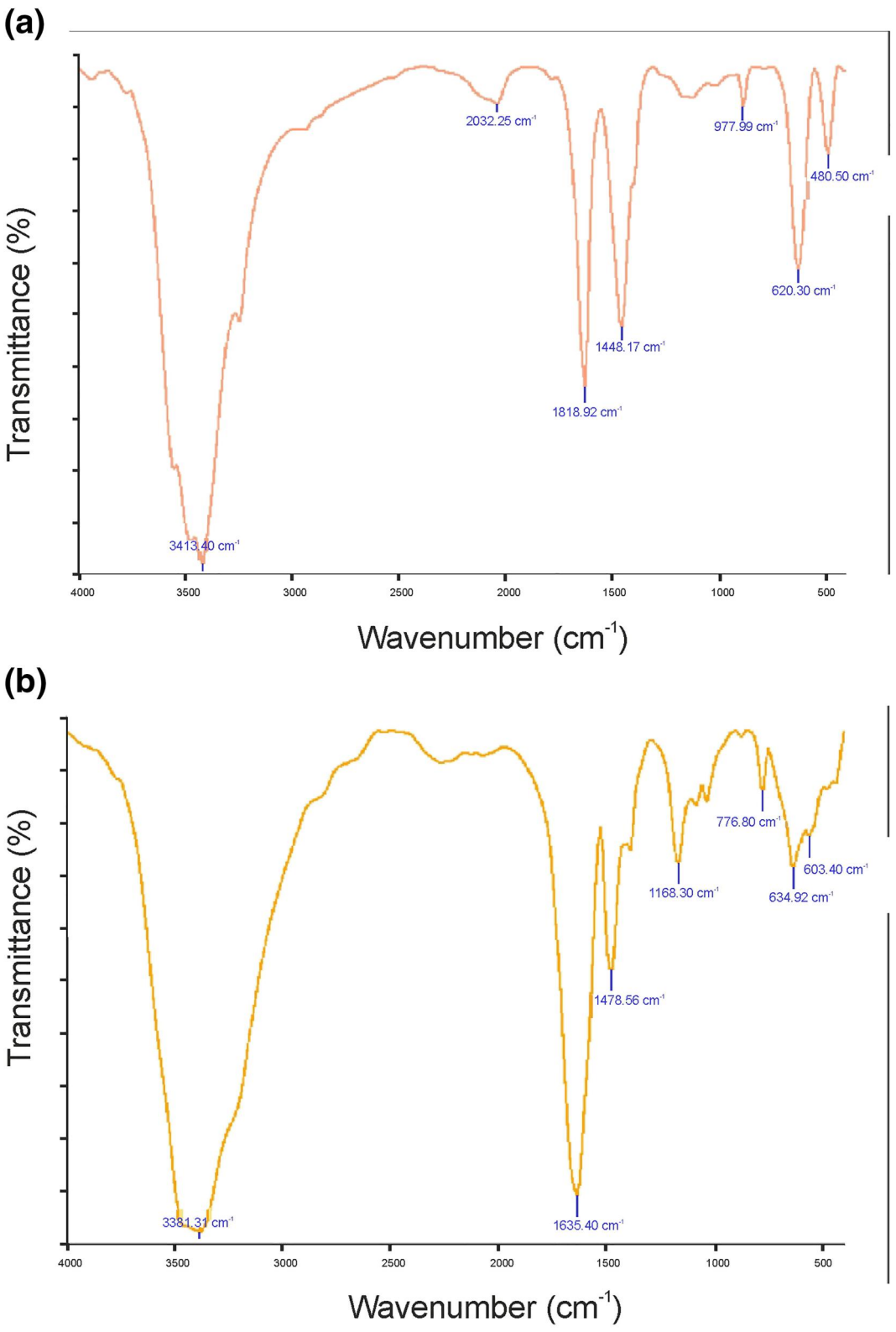

FIGURE 2 Fourier transform infrared spectrum of Mg-Al layered double hydroxide (LDH) (a) and Fe@Mg-Al LDH (b)

the sample solution after finishing the contact time with the adsorbent (mg L^{-1}), M is the adsorbent mass (g), V is the sample solution volume (L), q_e is the amount of adsorbent (mg g^{-1}) and R (%) is the percentage of the adsorption.

2.3.1 | pH

Different pHs were selected from 2 to 9 to obtain the optimal pH value using a buffer solution and 0.1 mol L^{-1} of HCl and NaOH solution [31, 32]. The 0.04 g of Fe@Mg-Al LDH was added to 25 ml of antimony solution with concentrations of 0.1 and 1.5 mg/L of EDTA ligand. The sample was placed on a magnetic stirrer at 20°C for 30 min. After centrifugation, the remaining ion concentration was determined by graphite furnace atomic absorption spectrometry (GFAAS).

2.3.2 | Amount of nanoadsorbent

To achieve the optimal amount of nanoadsorbent, the range of 0.005–0.05 g of nanoadsorbent was added to 25 ml of 0.1 mg/L antimony solution and 1.5 mg/L of EDTA ligand, which was stabilised at pH = 8 using a buffer. It was then placed on a magnetic stirrer for 30 min. The remaining ion concentration was then determined by GFAAS.

2.3.3 | Time

For the effect of time on the removal of antimony, a phosphate buffer solution with pH = 8 was used to stabilise a 0.1 mg/L of antimony solution and 1.5 mg/L of EDTA ligand. Then, 0.025 g of nanoadsorbent was added to the solution, and it was placed on a magnetic stirrer at different times for 1 to 30 min at 25°C. The remaining antimony ion concentration was then determined by GFAAS.

2.3.4 | Ligand

The effect of the amount of EDTA ligand on the removal of antimony was investigated. The samples containing EDTA ligand were prepared with a concentration of 0.05, 0.25, 0.5, 0.75, 1, 1.2, and 1.5 mg/L with pH constant at 8. The samples were placed on a magnetic stirrer at an optimal time of 25 min at room temperature, adding the optimal amount of 0.025 g of adsorbent. After centrifugation, the remaining ion concentration was determined by GFAAS.

2.3.5 | Solution volume

The effect of solution volume was studied on the removal of antimony for the determination of the enrichment factor and the maximum sample volume on the removal of antimony metal ions. Solutions with volumes of 25, 40, 50, 100, 250, and 200 ml of 0.1 mg/L antimony solution and the optimal amount of ligand were stabilised at pH = 8. They were then mixed with a 0.025 g of the nanoadsorbent on a magnetic stirrer at room temperature for 25 min. The remaining antimony ion concentration was determined using GFAAS.

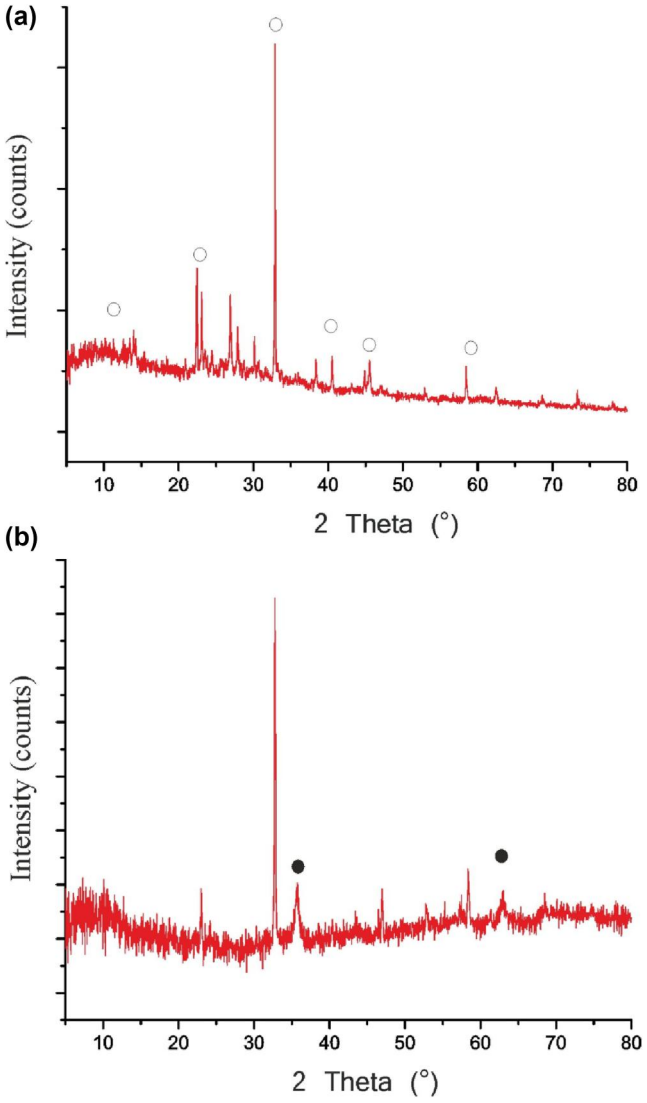

FIGURE 3 X-ray diffraction (XRD) pattern of Mg-Al layered double hydroxide (LDH) (a) and Fe@Mg-Al LDH (b)

2.3.6 | Temperature

In optimal conditions, the temperatures of 10, 15, 20, 25, 30, and 35°C were studied for antimony ions extractions with the refrigerated incubator shaker apparatus. The remaining ion concentration was determined by GFAAS.

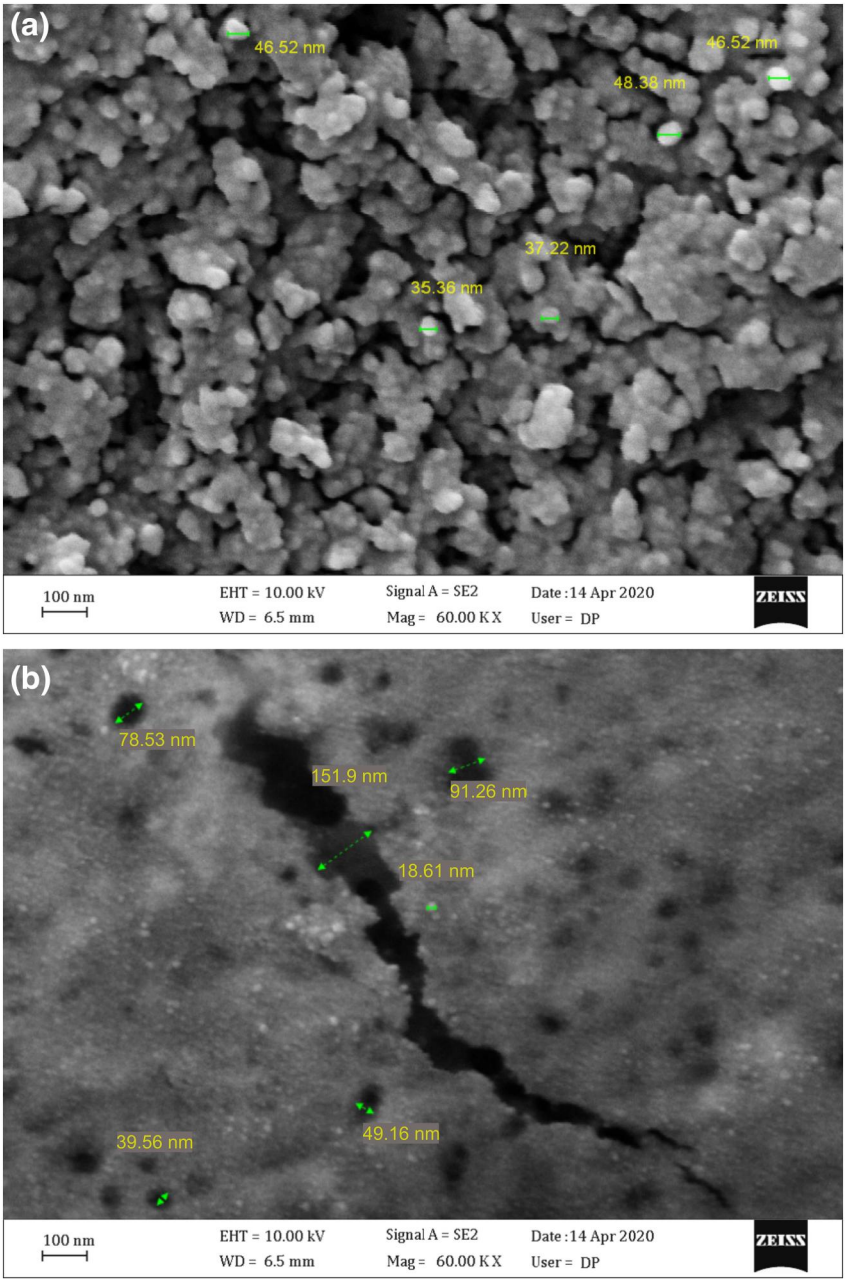

FIGURE 4 Field emission scanning electron microscopy image of Mg-Al layered double hydroxide (LDH) (a) and Fe@Mg-Al LDH (b) nanoparticles

3 | RESULT AND DISCUSSION

3.1 | Characterisation of adsorbent

FTIR analysis was seen in Figure 2. The wavenumbers ranged from 3413.4 to 3381.31 cm^{-1}, which were related to the stretching vibration of OH. The wavenumbers 1618.92 and 1635.40 cm^{-1} were created due to the vibrations of the water molecules. The appeared peaks between 500 and 800 cm^{-1} were related to the chemical bond between oxygen, Al-O, and Mg-O [7, 8]. The broad peak of about 603 cm^{-1} in Figure 2b corresponds to the bending vibration associated with Fe-O, which is not present in the spectrum of Figure 2a [33, 34]. This peak indicates the magnetisation of Mg-Al LDH.

As can be seen in Figure 3a,b, XRD was related to the first phase of Mg-Al LDH and the final phase of Fe@Mg-Al LDH, respectively. In Figure 3a, the position of the (003) plane corresponds to the basal spacing of Mg-Al LDH was appeared in $2\theta = 11.26°$ with 7.85 Å. The peaks identified in the pattern of Figure 3a are related to the hydrotalcite structure. The two additional peaks observed in the Fe@Mg-Al LDH pattern (Figure 3b) are due to the magnetisation of the adsorbent. Besides, due to the reduction of sharper peaks in Figure 3b, it

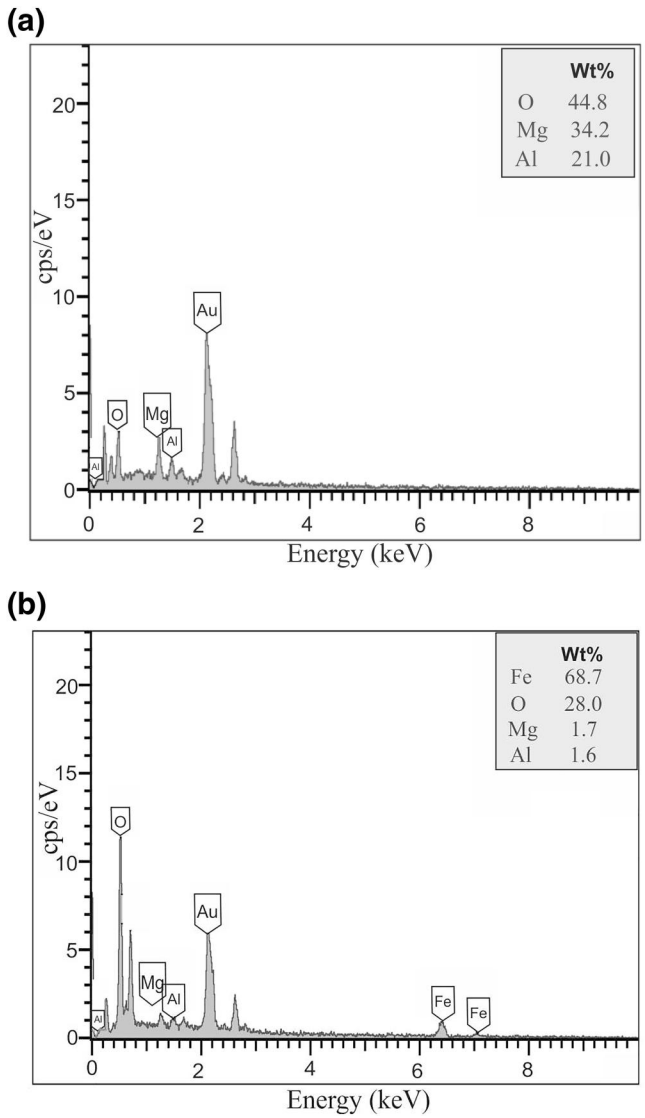

FIGURE 5 Energy dispersive X-ray spectroscopy (EDS) of Mg-Al layered double hydroxide (LDH) (a) and Fe@Mg-Al LDH (b) nanoparticles

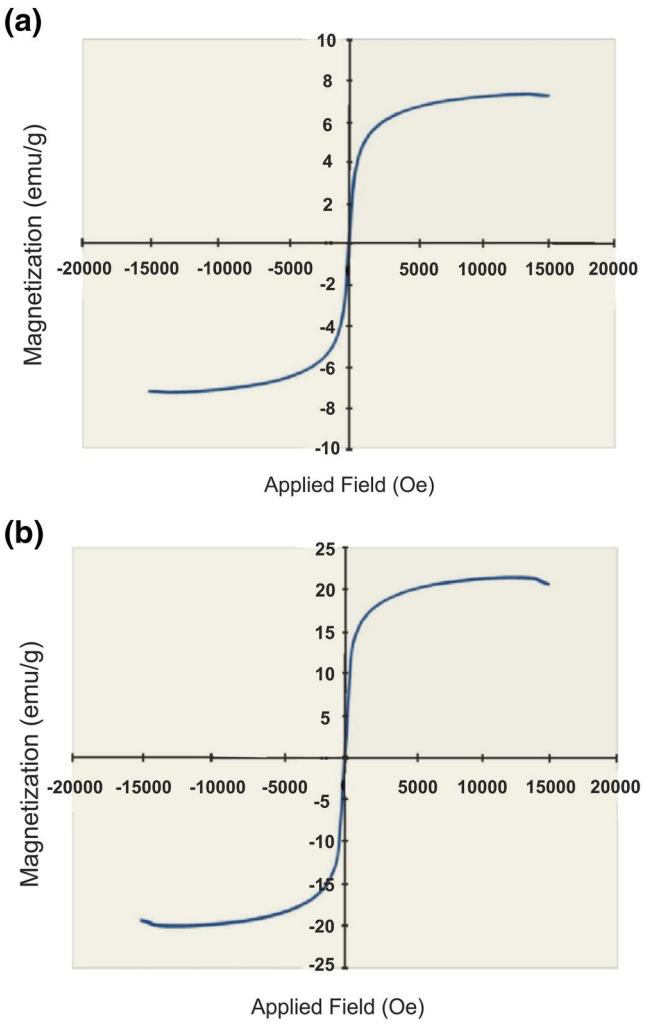

FIGURE 6 Vibrating sample magnetometer magnetisation curve of Mg-Al (a) and Fe@Mg-Al (b) LDH nanoparticles

can be seen that the crystallisation of the adsorbent decreased after the addition of Fe to Mg-Al LDH. [7, 35].

Figure 4a,b shows the field emission scanning electron microscopy (FESEM) images of Mg-Al LDH and Fe@Mg-Al LDH. Figure 4a is related to the LDH containing Mg-Al and the particles are displayed with 35–46 nm of sizes. Figure 4b is related to LDH containing Fe@Mg-Al and the signed points are shown with 39–151 nm and the iron element is quite clear.

Figure 5a,b is related to the EDS analysis and it shows the first phase of LDH contains Mg, Al, and O (Figure 5a), and the second phase of LDH contains Mg, Al, O, and Fe (Figure 5b).

Figure 6a,b is related to the VSM analysis of Mg-Al LDH and Fe@Mg-Al LDH. The saturation magnetisation of Mg-Al and Fe@Mg-Al LDH are shown as 6 and 18 emv/g, respectively. This increase in magnetisation was due to the addition of iron nanoparticles to Mg-Al LDH.

3.2 | The effect of pH on the removal of antimony

The adsorption of antimony with Fe@Mg-Al LDH depends on the pH of the nanocomposite surface. As observed in Figure 7, the pHzpc (zero point of charge) of Fe@Mg-Al LDH was 8. With a lower pH value than 8 for Fe@Mg-Al LDH, the hydroxyl groups of the Fe@Mg-Al LDH surface were protonated which increased the positive change on the surface. At this time, electrostatic repulsion is created between the Fe@Mg-Al LDH and antimony metal cations, resulting in a less removal capacity of antimony metal. At a higher pH value than 8, the hydroxyl groups of the Fe@Mg-Al LDH surface were deprotonated which increased the negative change on the surface and the tendency to adsorb antimony metal cations increases through electrostatic attraction. However, at higher pHs and excess OH^-, the possibility of precipitation and formation of the hydroxylated complexes of antimony increases [36, 37]. As can be seen from the diagram (Figure 8), at acidic pHs, the Fe@Mg-Al LDH surface has a high positive

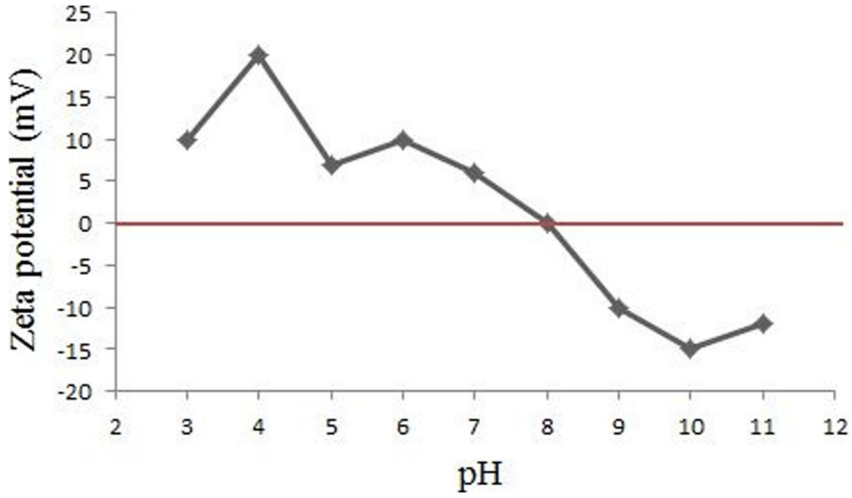

FIGURE 7 The Zeta potentials of Fe@Mg-Al energy dispersive X-ray spectroscopy (EDS) in various pH

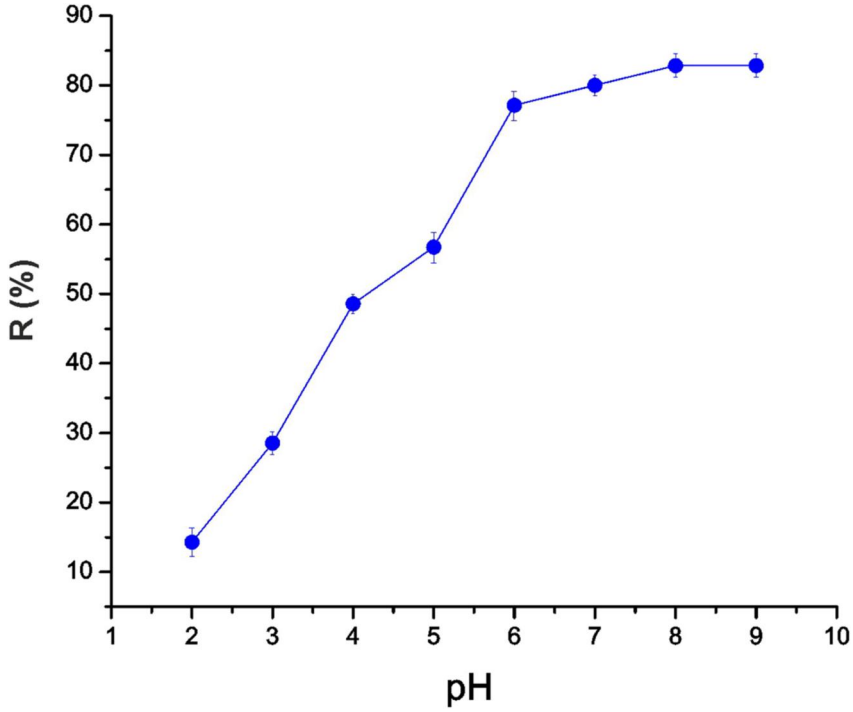

FIGURE 8 The effect of pH on the removal of antimony by Fe@Mg-Al energy dispersive X-ray spectroscopy (EDS; 0.04 g of Fe@Mg-Al LDH, 25 ml of antimony solution with 0.1 mg/L concentration, 1.5 mg/L of ethylenediaminetetraacetic acid, 20°C for 30 min)

charge and the repulsive force prevents antimony metal cations from being adsorbed on it and the extraction process rate is low. As the pH increases and approaches 7, the positive charge on the surface and H^+ ion in solution decreases and antimony metal cations are more easily adsorbed [7, 38, 39]. At pH = 8, the highest adsorption of antimony metal cations was observed with the nanocomposite surface.

3.3 | The effect of the amount of nanoadsorbent on the removal of antimony ions

The 0.025 g amount of nanoadsorbent was found for the maximum adsorption of antimony ions with Fe@Mg-Al LDH (Figure 9).

3.4 | The effect of time on the removal of antimony

As shown in Figure 10, with the increase in time, the efficiency increased and the curve has a steep slope up to 25 min. The time of 25 min is the equilibrium time for the adsorption of Sb(III) ions by Fe@Mg-Al LDH, which is the optimal time due to time savings and no significant difference between 25 and 30 min [40].

3.5 | Effect of the amount of EDTA ligand on the removal of antimony

As shown in Figure 11, with increasing the concentration of the ligand to 1 mg/L, the efficiency increased because the

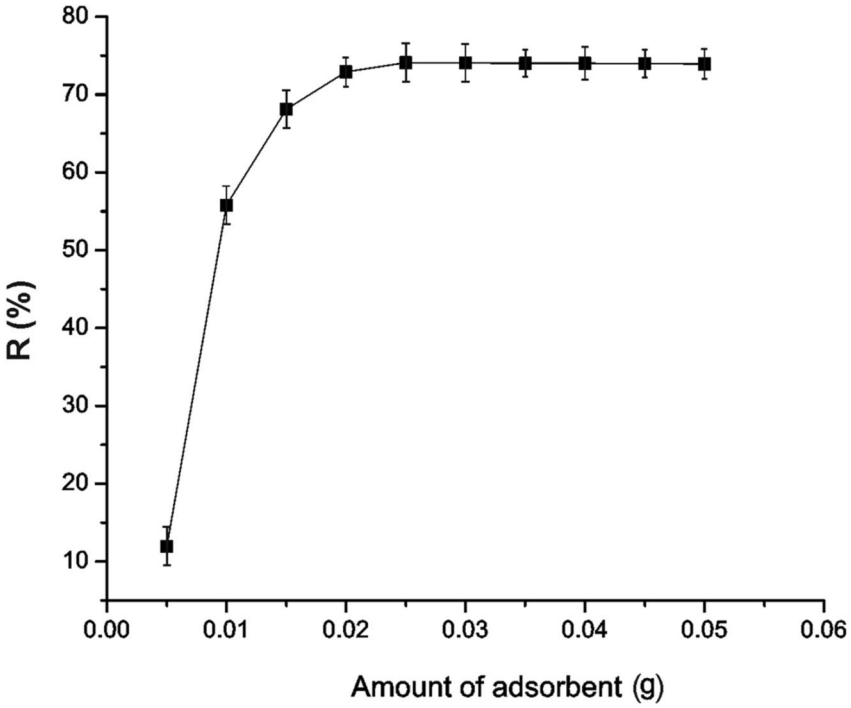

FIGURE 9 Efficiency rate by the amount of adsorbent (pH = 8, 25 ml of antimony solution with 0.1 mg/L concentration, 1.5 mg/L of ethylenediaminetetraacetic acid, 20°C for 30 min)

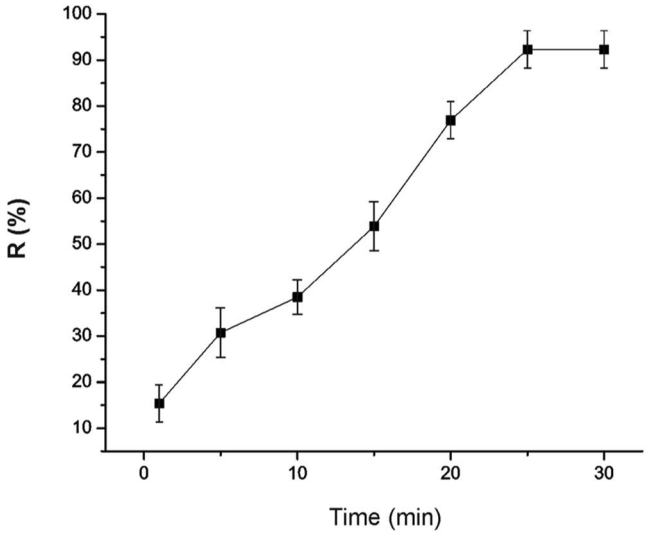

FIGURE 10 Effect of time on the antimony ions removal (0.025 g of Fe@Mg-Al LDH, pH = 8, 25 ml of antimony solution with 0.1 mg/L concentration, 1.5 mg/L of ethylenediaminetetraacetic acid, 20°C)

ligand formed a complex with antimony. However, the lack of change in the efficiency after the concentration of 1 mg/L could be attributed to the saturation of the nanoadsorbent active surface.

3.6 | The effect of solution volume

As can be seen in Figure 12, with an increase in volume sample (25 ml), the recovery extraction is decreased. This is probably explained by the limitation of contact between the antimony ions and nanoadsorbent sites [41, 42].

3.7 | Temperature effect

The purpose of measuring the temperature is to investigate the antimony ion extractions and thermodynamic parameters. As can be seen in Figure 13, the extraction efficiency increased with increasing temperature up to 30°C. As the temperature rises, the activity of the metal ions in the solution increases, and the chances of colliding with the empty sites of nanoadsorbent increase [43].

3.8 | Interfering ions

Interfering cations are referred to as ions that cause a change of up to 5% in the absorbance signal of the goal ion. The effect of interfering ions was investigated on the removal of antimony. Other ions were used in addition to the antimony ions to prove the adequacy of the nanoadsorbent. For this purpose, different concentrations of interfering ions (presented in Table 1) were added to the optimal solution with the nanoadsorbent. After the extraction process and centrifugation, the remaining ion concentration was determined by GFAAS. The obtained result displayed that the addition of the cations does not have considerable interference in the determination and removal of antimony ions [44].

3.9 | Elution solvent selection

The type of solvent selected for elution and desorption of antimony metal ions is one of the main factors that has a great impact on the metal removal system. In this study, various elution solvents have been used in combination and separately,

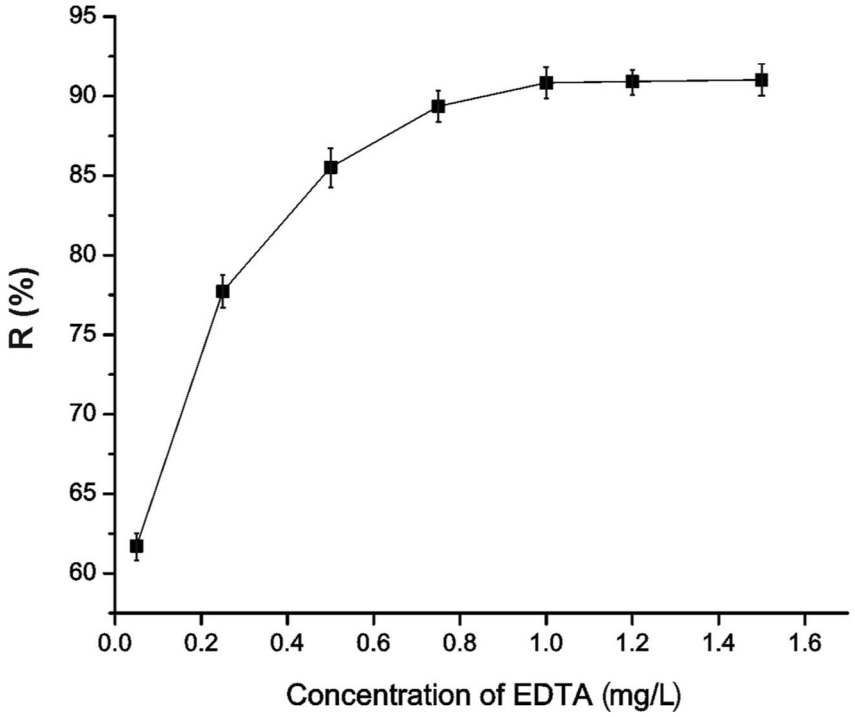

FIGURE 11 Efficiency by the ligand concentration (0.025 g of Fe@Mg-Al layered double hydroxide, pH = 8, 25 ml of antimony solution with 0.1 mg/L concentration, 20°C for 25 min)

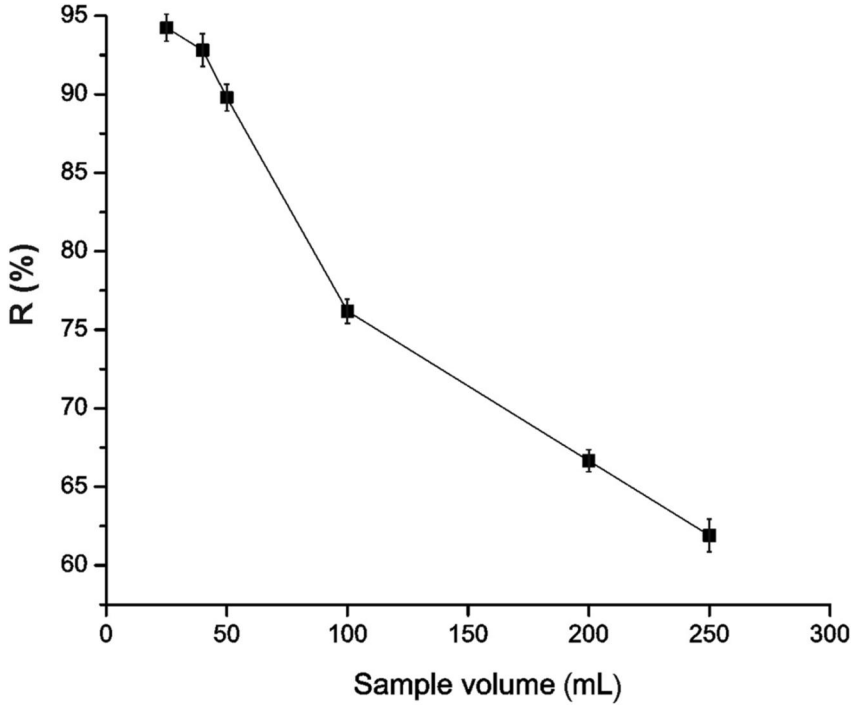

FIGURE 12 Effect of solution volume on the removal of antimony ions (0.025 g of Fe@Mg-Al layered double hydroxide, pH = 8, antimony solution with 0.1 mg/L concentration, 1 mg/L of ethylenediaminetetraacetic acid, 20°C for 25 min)

and the optimal solvent for antimony metal ions removal has been selected (Figure 14). Considering the maximum antimony extraction with acidic methanol, it was selected for the desorption of antimony metal ions with the ideal balance created between the Fe@Mg-Al LDH and this solvent. Furthermore, the volume of elution solvent was investigated with a volume range of 10–35 ml of optimum elution solvent. The result is shown in Figure 15 that the goal volume for desorption of antimony metal ions from Fe@Mg-Al LDH was found to be 25 ml [45, 46].

3.10 | Replicability

To achieve the standard deviation method as an important analytical factor, antimony metal ions were extracted and

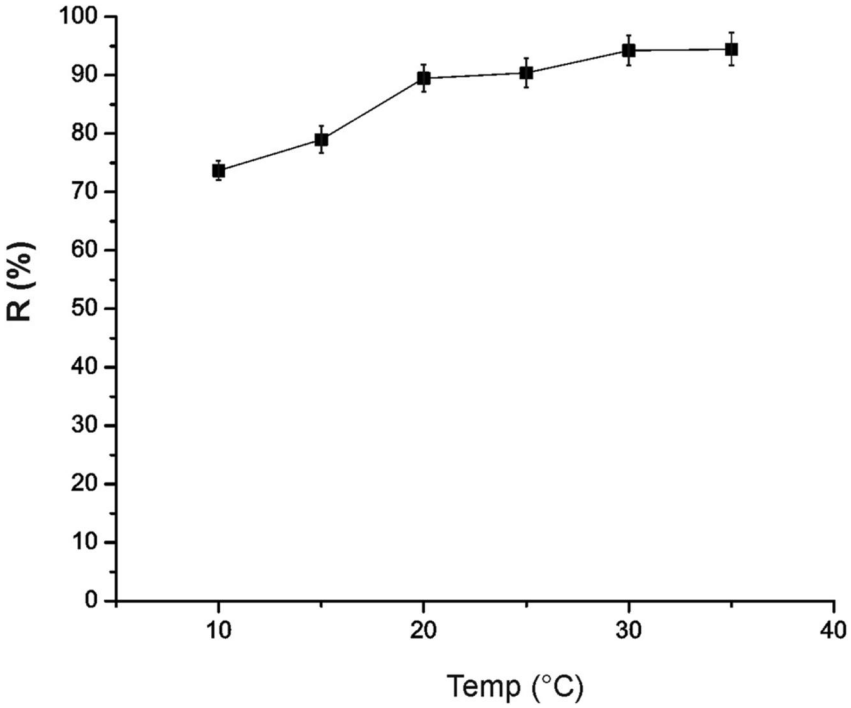

FIGURE 13 Temperature effect on the removal of antimony ions (0.025 g of Fe@Mg-Al LDH, pH = 8, 25 ml of antimony solution with 0.1 mg/L concentration, 1 mg/L of ethylenediaminetetraacetic acid, 25 min)

TABLE 1 The effect of different concentrations of interfering ions on the adsorption efficiency of 0.1 mg/L of antimony and 1 mg/L of ethylenediaminetetraacetic acid ligand ($n = 3$)

Interfering ion	Added (μg/L)	Recovery (%)
Cr^{3+}	27.45	90.85
Ni^{2+}	30.78	89.74
Cu^{2+}	31.08	89.64
Pb^{2+}	26.04	91.32
Na^{+}	34.29	88.57
Ca^{2+}	32.28	89.24
Zn^{2+}	33.15	88.95
Ag^{+}	26.34	91.22
K^{+}	29.82	90.06
Co^{2+}	37.74	87.42
Al^{3+}	29.83	90.39

removed by nanoadsorbent five times using the method presented in this study. The remaining ions concentration was determined and a calibration curve was drawn. The standard deviation value of the method was found at 7.92%. It was acknowledged that the method was replicable.

3.11 | Real samples analysis

To evaluate the accuracy of the proposed method, the standard addition method has been used for different real samples (well water, snow water, rainwater, and seawater). These samples were purified with nitric acid after passing through filtration and storage in containers. The solutions were in contact with 0.025 g of nanoadsorbent at 30°C and pH = 8 for 25 min. The adsorption ions and efficiency were investigated after the separation and signal reading by GFAAS (Table 2). The results in Table 2 show that Fe@Mg-Al LDH is effective in preconcentration and designation of antimony ions in a complex matrix, for example, various aqueous samples.

3.12 | Reusability study of the Fe@Mg-Al LDH

To study the Fe@Mg-Al LDH sorbent reusability, the experiments of antimony ions sorption-desorption were carried out 6 cycles repeatedly via mentioned processes. The 25 ml of 0.1 mg/L solutions of antimony ions and 1 mg/L of EDTA were prepared at pH = 8 and then 0.025 g of Fe@Mg-Al LDH was added and stirred for 25 min at 30°C, then centrifuged and finally washed with 25 ml of acidic methanol, and then the concentration of antimony ions in solution was monitored by GFAAS. Then, the Fe@Mg-Al LDH was washed with water/ethanol and dried and re-tested for the second time according to the mentioned process. This experiment was carried out five times, and the obtained results display that it is possible to apply the Fe@Mg-Al LDH three times.

3.13 | Study of isotherms

Freundlich, Langmuir, and Temkin isotherms were used to achieve the adsorption model. The amount of adsorbed

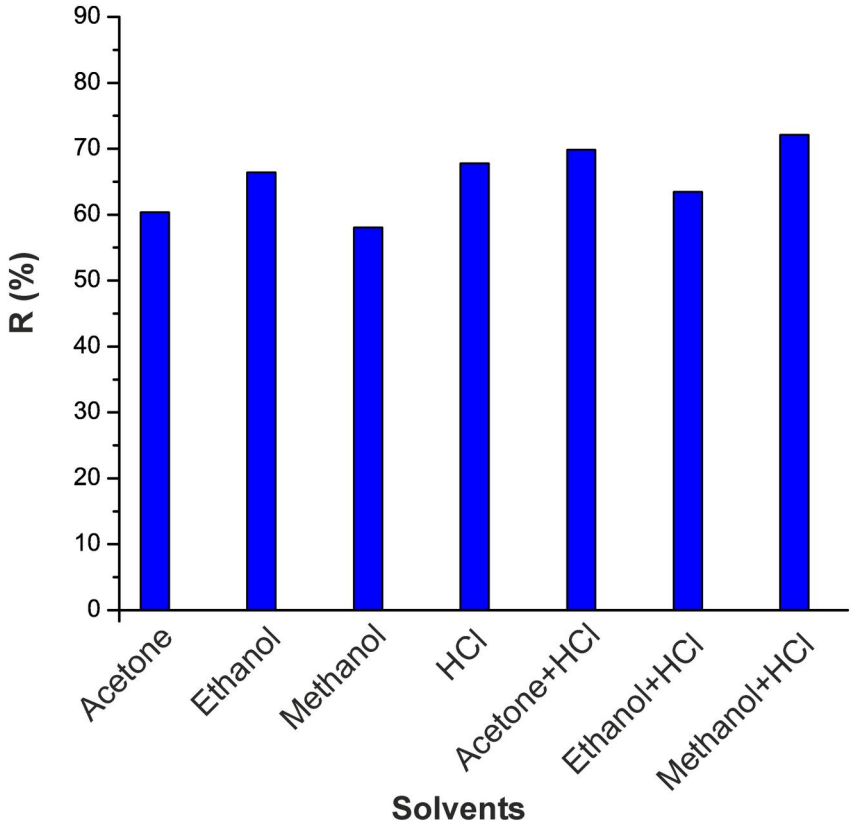

FIGURE 14 Effect of elution solvent on antimony metal ions adsorption

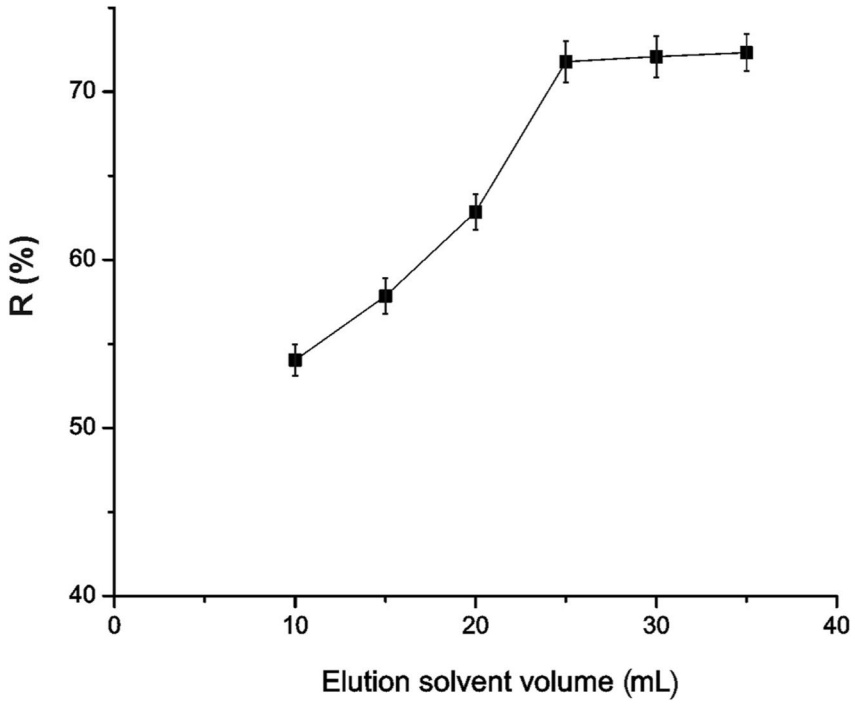

FIGURE 15 Effect of elution solvent volume

antimony ions at equilibrium q_e (mg/g) was calculated by Equation 2). Adsorption isotherms are equations for describing the equilibrium state of the adsorbed component between the solid and fluid phases. At this stage, the experimental data on adsorption equilibrium with Freundlich, Langmuir, and Temkin isotherms were examined. The equations for isotherm models of Langmuir, Temkin, and Freundlich are as follows, respectively [47, 48].

$$\frac{C_e}{q_e} = \frac{1}{Q_0 b} + \frac{C_e}{Q_0} \quad (3)$$

$$q_e = B \ln k_T + B \mathrm{Ln}\, C_e \quad (4)$$

$$\log q_e = \log K_f + \frac{1}{n} \log C_e \quad (5)$$

where Q_0 is the highest antimony ions sorption capacity at Fe@Mg-Al LDH (mg/g) and b is the constant of the Langmuir Equation (L/mg), k_T (L/g) and B (J/mol) are the constants of the Temkin Equation, K_f ((mg/g)·(L/mg)$^{1/n}$) and n are the constants of the Freundlich Equation, C_e (mg/L) is the concentration of the adsorbate in the liquid phase after reaching equilibrium, and q_e (mg/L) is the amount of the adsorbate per unit mass of Fe@Mg-Al LDH [49].

The parameters of isotherm models are deposited in Table 3. The correlation coefficient of Langmuir isotherm for antimony ions is 0.917, while this value of the Freundlich and Temkin isotherms is 0.808 and 0.847, respectively. The results show that the Langmuir model can be considered as a monolayer adsorption mechanism of antimony metal ions on the Fe@Mg-Al LDH. Similar results were observed in the adsorption isotherm studies of various pollutant-adsorbent systems [50–53].

TABLE 2 Recovery of antimony ions was added to 1000 ml of different water samples (pH = 8)

Sample	Antimony added (μg)	Antimony determined (μg)
Well water	0.0	2.12 (0.401)[a]
	10.0	12.4 (0.0502)
Snow water	0.0	N.D.[b]
	10.0	12.1 (0.710)
Rain water	0.0	0.890 (2.17)
	10.0	11.4 (0.171)
Sea water	0.0	8.74 (0.243)
	10.0	18.9 (2.67)

[a]Values in parentheses are RSDs based on five individual replicate analyses.
[b]Not Detection.

3.14 | Determination of thermodynamic parameters

Thermodynamic parameters include changes in Gibbs free energy change (ΔG), enthalpy change (ΔH), and entropy change (ΔS), which are the most important features of an adsorption process for practical applications. Thermodynamic equations help to better understand the process of adsorption, that is, to increase the adsorption efficiency. According to Table 4, since all ΔGs were positive for antimony ions, it could be concluded that all adsorption processes by the Fe@Mg-Al LDH were non-spontaneous [54, 55]. Additionally, if the ΔG was between 0 and 20, the adsorption processes were chemical. The positive enthalpy change of adsorption reactions on the Fe@Mg-Al LDH indicated that these processes were endothermic. The entropy changes in adsorption by Fe@Mg-Al LDH were positive, indicating that the degree of freedom at the solid-solution phase in adsorption increased.

The standard free energy change (ΔG^0) can be calculated from the following equation 6:

$$\Delta \mathrm{G}^0 = -RT \mathrm{Ln} K \quad (6)$$

where R is the universal gas constant (8.314 J/mol K), T is the temperature (K) and K is the sorption equilibrium constant. The standard entropy change ($\Delta \mathrm{S}^0$) can be calculated according to the following equation or by plotting ln$K$ versus $1/T$ $\left(\ln K = \frac{\Delta S^0}{R} - \frac{\Delta H^0}{RT}\right)$ [56, 57].

$$\Delta \mathrm{G}^0 = \Delta \mathrm{H}^0 - \mathrm{T} \Delta \mathrm{S}^0 \quad (7)$$

3.15 | Comparison of the removal of antimony (III) by different adsorbents

Table 5 presents the removal of antimony (III) by different adsorbents, which is compared with the method provided in this study. As can be seen, the adsorbent presented in this study has advantages that contain the best adsorption time and the amount of adsorbent was much less than that of

TABLE 3 Freundlich, Langmuir, and Temkin isotherms constants for the adsorption of antimony ions by Fe@Mg-Al LDH

Freundlich isotherm			Langmuir isotherm			Temkin isotherm		
n	K_f ([mg/g]·[L/mg]$^{1/n}$)	R^2	Q_0 (mg/g)	b (L/mg)	R^2	k_t (L/g)	B (J/mol)	R^2
1.60	0.948	0.808	160	0.102	0.917	0.245	0.0660	0.847

TABLE 4 Thermodynamic parameters

T (Kelvin)	ln$K$	ΔG^0 (kJ/mol)	ΔH^0 (kJ/mol)	ΔS^0 (kJ/mol K)
283	−1.65	3.90	14.3	0.0370
293	−1.45	3.53		
303	−1.20	3.04		

TABLE 5 Comparison of the removal of antimony (III) by different adsorbents

Adsorbent	Sb oxidation State	pH	T (K)	Adsorbent dose (g/L)	Contact time (min)	Removal rate (%)	Ref
Haematite modified magnetic nanoparticles	Sb(III)	4.1	298	0.1	120	>95.5	[58]
Fe_2O_3 modified carbon nanotubes	Sb(III)	7	298	0.5	120	99.97	[59]
Fe_2O_3/Fe_3O_4/C prepared with bamboo template	Sb(III)	7	298	2	-	>90	[60]
Fe@Mg-Al LDH	Sb(III)	8	303	0.025	25	>94.43	This work

Abbreviation: LDH, layered double hydroxide.

previously published adsorbents for the removal of antimony (III) [58–60]. In this study, the use of EDTA causes more stability of antimony ions in solution and can increase the adsorption efficiency. Also, in the formation of EDTA complex and metal ions, it is possible to be located between the LDH layers, which increases the adsorption efficiency [61].

4 | CONCLUSION

This study was conducted with the aim of providing a simple, effective, repeatable, and inexpensive method to remove antimony metal ions. According to the findings of the study, the Fe@Mg-Al LDH adsorbent has a good ability to remove antimony ions from various water samples with near-neutral pH. In this method, with the minimum amount of Fe@Mg-Al LDH (0.025 g), good results have been obtained for the removal of antimony metal ions with high adsorption capacity (160.15 mg/g). The results of the study of adsorption isotherm models demonstrate the adaptation of Langmuir adsorption mechanism for antimony metal ion adsorption in the form of complex formation with EDTA as a monolayer on the Fe@Mg-Al LDH. It can also be acknowledged that the presence of interfering ions does not have much effect on ions extraction. Besides, the used method was replicable and had positive results on real samples. Also, based on the study of thermodynamic parameters, the process of extraction of antimony metal ions by the Fe@Mg-Al LDH was non-spontaneous and endothermic.

ACKNOWLEDGEMENTS

This study was supported by the Islamic Azad University, Varamin Pishva Branch.

CONFLICT OF INTEREST

The authors declare no conflict of interests.

DATA AVAILABILITY STATEMENT

Data openly available in a public repository that issues datasets with DOIs.

ORCID

Ali Moghimi https://orcid.org/0000-0002-4196-5023

REFERENCES

1. Duman, O., Ayranci, E.: Attachment of benzo-crown ethers onto activated carbon cloth to enhance the removal of chromium, cobalt and nickel ions from aqueous solutions by adsorption. J. Hazard. Mater. 176, 231–238 (2010). https://doi.org/10.1016/j.jhazmat.2009.11.018
2. Pintor, A.M.A., et al.: Removal of antimony from water by iron-coated cork granulates. Sep. Purif. Technol. 233, 116020 (2020)
3. Faustova, Z.V., Slizhov, Y.G., Matveeva, T.N.: Synthesis of surface-porous sorbents based on silicon dioxide and studying their adsorption properties. Russ. J. Appl. Chem. 93, 1211–1220 (2020). https://doi.org/10.1134/S1070427220080145
4. Sayadi, M.H., Rashki, O., Shahri, E.: Application of modified Spirulina platensis and *Chlorella vulgaris* powder on the adsorption of heavy metals from aqueous solutions. J. Environ. Chem. Eng. 7, 103169 (2019)
5. Farooghi, A., et al.: An efficient removal of lead from aqueous solutions using $FeNi_3$@ SiO_2 magnetic nanocomposite. Surf. Interfaces. 10, 58–64 (2018)
6. Karimi, P., et al.: Arsenic removal from mining effluents using plant-mediated, green-synthesized iron nanoparticles. Processes. 7, 759 (2019)
7. Abniki, M., Moghimi, A., Azizinejad, F.: Fabrication of bio-nanocomposite based on LDH using biopolymer of gum Arabic and chitosan-coating for sustained drug-release. J. Serbian Chem. Soc. 85, 1223–1235 (2020)
8. Abniki, M., Moghimi, A., Azizinejad, F.: Synthesis of calcium-layered double hydroxide based nanohybrid for controlled release of an anti-inflammatory drug. J. Chin. Chem. Soc. 68, 343–352 (2021)
9. Xue, B., et al.: Layered Double Hydroxide-Based Nanocarriers for Drug Delivery. pharmaceutics 6(2), 298–332. (2014). https://doi.org/10.3390/pharmaceutics6020298
10. Carlino, S., Hudson, M.J.: A thermal decomposition study on the intercalation of tris-(oxalato) ferrate (III) trihydrate into a layered (Mg/Al) double hydroxide. Solid State Ionics. 110, 153–161 (1998)
11. Yu, S., et al.: Rational design of carbonaceous nanofiber/Ni-Al layered double hydroxide nanocomposites for high-efficiency removal of heavy metals from aqueous solutions. Environ. Pollut. 242, 1–11 (2018)
12. Onishi, W., et al.: Photoluminescence and photostability of YVO4: Eu^{3+} nanoparticle/layered double hydroxide multilayer films prepared via layer-by-layer assembly. J. Lumin. 175, 71–77 (2016)
13. Duman, O., et al.: Removal of triphenylmethane and reactive azo dyes from aqueous solution by magnetic carbon nanotube-κ-carrageenan-Fe_3O_4 nanocomposite. J. Alloys Compd. 687, 370–383 (2016). https://doi.org/10.1016/j.jallcom.2016.06.160
14. Duman, O., et al.: Carbon nanotube-based magnetic and non-magnetic adsorbents for the high-efficiency removal of diquat dibromide herbicide from water: OMWCNT, OMWCNT-Fe_3O_4 and OMWCNT-κ-carrageenan-Fe_3O_4 nanocomposites. Environ. Pollut. 244, 723–732 (2019). https://doi.org/10.1016/j.envpol.2018.10.071
15. Duman, O., et al.: Synthesis of magnetic oxidized multiwalled carbon nanotube-κ-carrageenan-Fe_3O_4 nanocomposite adsorbent and its application in cationic Methylene Blue dye adsorption. Carbohydr. Polym. 147, 79–88 (2016). https://doi.org/10.1016/j.carbpol.2016.03.099

16. Sereshti, H., et al.: Nanosorbent-based solid phase microextraction techniques for the monitoring of emerging organic contaminants in water and wastewater samples. Microchim. Acta. 187, 541 (2020). https://doi.org/10.1007/s00604-020-04527-w
17. Nouri, N., et al.: Overview of nanosorbents used in solid phase extraction techniques for the monitoring of emerging organic contaminants in water and wastewater samples. Trends Environ. Anal. Chem. 25, e00081 (2020). https://doi.org/10.1016/j.teac.2020.e00081
18. Li, L., et al.: Fe_3O_4 core/layered double hydroxide shell nanocomposite: versatile magnetic matrix for anionic functional materials. Angew. Chem. Int. Ed. 48, 5888–5892 (2009)
19. Mitchell, M.C., et al.: Microchip-based synthesis and total analysis systems (μSYNTAS): chemical microprocessing for generation and analysis of compound libraries. J. Chem. Soc. Perkin Trans. 1, 514–518 (2001)
20. Pourshamsi, T., Amri, F., Abniki, M.: A comprehensive review on application of the syringe in liquid-and solid-phase microextraction methods. J. Iran. Chem. Soc. 18 245–264 (2020). https://doi.org/10.1007/s13738-020-02025-7
21. Rezaei, S., et al.: Optimization by response surface methodology of the adsorption of anionic dye on superparamagnetic clay/Maghemite nanocomposite. Russ. J. Appl. Chem. 94, 533–548 (2021). https://doi.org/10.1134/S1070427221040145
22. Abniki, M., Moghimi, A.: Synthesis of chitosan functionalized magnetic carbon nanotubes for dispersive solid-phase extraction of bromocresol green. Micro & Nano Lett. 16, 455–462 (2021)
23. Moghimi, A., et al.: Solid phase extraction of Hg (II) in water samples by nano-Fe. Int. J. Bio-Inorg. Hybr. Nanomater. 8, 163 (2019)
24. Song, Y., et al.: The application of EDTA in drug delivery systems: doxorubicin liposomes loaded via NH_4EDTA gradient. Int. J. Nanomed. 9, 3611 (2014)
25. Ezzeddine, Z., et al.: Divalent heavy metals adsorption onto different types of EDTA-modified mesoporous materials: effectiveness and complexation rate. Micropor. Mesopor. Mat. 212, 125–136 (2015)
26. Kao, F.-C., et al.: The application of nanogenerators and piezoelectricity in osteogenesis. Sci. Technol. Adv. Mater. 20, 1103–1117 (2019)
27. Vitha, M.F.: Spectroscopy: Principles and Instrumentation. John Wiley & Sons (2018)
28. Xu, Z., et al.: Combined toxicity of soil antimony and cadmium on earthworm Eisenia fetida: accumulation, biomarker responses and joint effect. J. Hazard. Mater. Lett. 2, 100018 (2021)
29. Bai, Y., Wu, F., Gong, Y.: Oxidation and adsorption of antimony (iii) from surface water using novel Al_2O_3-supported Fe–Mn binary oxide nanoparticles: effectiveness, dynamic quantitative mechanisms, and life cycle analysis. Environ. Sci. Nano. 7, 3047–3061 (2020)
30. Guo, X., Wu, Z., He, M.: Removal of antimony (V) and antimony (III) from drinking water by coagulation–flocculation–sedimentation (CFS). Water Res. 43, 4327–4335 (2009)
31. Moghimi, A., Abniki, M.: The dispersive solid-phase extraction of fluoxetine drug from biological samples by the Amine-functionalized carbon nanotubes with HPLC method. Chem. Methodol. 5, 250 (2021)
32. Sayadi, M.H., et al.: Bio-synthesis of palladium nanoparticle using Spirulina platensis alga extract and its application as adsorbent. Surf. Interfaces. 10, 136–143 (2018)
33. Safa, F., Alinezhad, Y.: Ternary nanocomposite of SiO2/Fe3O4/Multi-Walled Carbon Nanotubes for Efficient Adsorption of Malachite Green: Response Surface Modeling, Equilibrium Isotherms and Kinetics. Equilib. Isotherms Kinet. Silicon. 12 1619–1637 (2019). https://doi.org/10.1007/s12633-019-00251-0
34. Moghimi, A., Abniki, M.: Removal and measurement of bromocresol purple dye in aqueous samples by β-cyclodextrin-modified magnetic carbon nanotube with dispersive solid-phase extraction technique. J. Color Sci. Technol. (2021). https://jcst.icrc.ac.ir/article_81773.html
35. Jung, I.-K., et al.: Efficient removal of iodide anion from aqueous solution with recyclable core-shell magnetic Fe_3O_4@ Mg/Al layered double hydroxide (LDH). Sci. Total Environ. 705, 135814 (2020)
36. Watkins, R., et al.: Investigations into the kinetics and thermodynamics of Sb (III) adsorption on goethite (α-FeOOH). J. colloid interface Sci. 303, 639–646 (2006)
37. Targan, Ş., Tirtom, V.N., Akkuş, B.: Removal of antimony (III) from aqueous solution by using grey and red Erzurum clay and application to the Gediz River sample. Int. Sch. Res. Notices. 2013 (2013). https://doi.org/10.1155/2013/962781
38. Yang, Q., et al.: In situ stabilization of the adsorbed Co_2^+ and Ni_2^+ in rice straw biochar based on LDH and its reutilization in the activation of peroxymonosulfate. J. Hazard. Mater. 416, 126215 (2021)
39. Soltani, R., et al.: A water-stable functionalized NiCo-LDH/MOF nanocomposite: green synthesis, characterization, and its environmental application for heavy metals adsorption. Arabian J. Chem. 14, 103052 (2021)
40. Shekari, H., et al.: Synthesis of nickel ferrite/titanium oxide magnetic nanocomposite and its use to remove hexavalent chromium from aqueous solutions. Surfaces Interfaces. 8, 199–205 (2017)
41. Krawczyk, M., Jeszka-Skowron, M.: Multiwalled carbon nanotubes as solid sorbent in dispersive micro solid-phase extraction for the sequential determination of cadmium and lead in water samples. Microchem. J. 126, 296–301 (2016)
42. Moghimi, A., Abniki, M.: Preconcentration and separation of ultra-trace Cu (II) with disks of octadecyl silica membrane modified nano-Fe_3O_4-encapsulated-dioctyl phthalate and linked-diethylenetriamine. Adv. J. Chem. Sect. A. 4, 78 (2021)
43. Chen, H., et al.: Hollow fiber liquid-phase microextraction of cadmium (II) using an ionic liquid as the extractant. Microchim. Acta. 181, 1455–1461 (2014)
44. Helzlsouer, K.J., et al.: Association between α-tocopherol, γ-tocopherol, selenium, and subsequent prostate cancer. J. Natl. Cancer Inst. 92(24), 2018–2023 (2000)
45. Zadeh, R.J., Sayadi, M.H., Rezaei, M.R.: Removal of 2,4-dichlorophenoxyacetic acid from aqueous solutions by modified magnetic nanoparticles with amino functional groups. J. Water Environ. Nanotechnol. 5, 147 (2020)
46. Zadeh, R.J., Sayadi, M.H., Rezaei, M.R.: Synthesis of Thiol modified magMCM-41 nanoparticles with rice husk ash as a robust, high effective, and recycling magnetic sorbent for the removal of herbicides. J. Environ. Chem. Eng. 9, 104804 (2021)
47. Abniki, M., Azizi, Z., Panahi, H.A.: Design of 3-aminophenol-grafted polymer-modified zinc sulphide nanoparticles as drug delivery system. IET Nanobiotechnology (2021). https://doi.org/10.1049/nbt2.12063
48. Siddique, M., et al.: Thermal-pressure-mediated hydrolysis of reactive blue 19 dye. J. Hazard. Mater. 172, 1007–1012 (2009)
49. Hosseini, R., Sayadi, M.H., Shekari, H.: Adsorption of nickel and chromium from aqueous solutions using copper oxide nanoparticles: adsorption isotherms, kinetic modeling, and thermodynamic studies. Avicenna J. Environ. Health Eng. 6, 66–74 (2019)
50. Duman, O., Tunc, S., Polat, T.G.: Adsorptive removal of triarylmethane dye (Basic Red 9) from aqueous solution by sepiolite as effective and low-cost adsorbent. Micropor. Mesopor. Mat. 210, 176–184 (2015)
51. Duman, O., et al.: Agar/κ-carrageenan composite hydrogel adsorbent for the removal of methylene blue from water. Int. J. Biol. Macromol. 160, 823–835 (2020)
52. Duman, O., Tunç, S., Polat, T.G.: Determination of adsorptive properties of expanded vermiculite for the removal of CI Basic Red 9 from aqueous solution: kinetic, isotherm and thermodynamic studies. Appl. Clay Sci. 109, 22–32 (2015)
53. Heidari, A., Sayadi, M., Atigh, Z.B.Q.: A comparative study of different materials (drinking water treatment sludge, nanoclay, and modified nanoclay) for simultaneous removal of hexavalent chromium and lead. Int. J. Environ. Sci. Technol., 18 3553–3570 (2021). https://doi.org/10.1007/s13762-020-03074-4
54. Khan, H., et al.: Adsorptive removal of acrylic acid from the aqueous environment using raw and chemically modified alumina: batch adsorption, kinetic, equilibrium and thermodynamic studies. J. Environ. Chem. Eng. 8, 103927 (2020)
55. Janighorban, M., et al.: Response surface methodology for optimizing Cd (II) adsorption onto a novel chemically changed nano Zn2Al-layer double hydroxide. Adv. J. Chem. Sect. A. 3, 701 (2020)

56. Kojima, Y., Yamaguchi, M.: Investigation on hydrogen dissociation pressure, heat of formation and strain energy of metal hydrides. J. Alloys Compd. 840, 155686 (2020)
57. Banjare, M.K., et al.: Inclusion complexation of novel synthesis amino acid based ionic liquids with β-cyclodextrin. J. Mol. Liq. 299, 112204 (2020)
58. Shan, C., Ma, Z., Tong, M.: Efficient removal of trace antimony (III) through adsorption by hematite modified magnetic nanoparticles. J. Hazard. Mater. 268, 229–236 (2014)
59. Yanqiu, L., et al.: Removal of antimony(III) from aqueous solution by graphene as an adsorbent. Chemical Engineering Journal 211 406–411 (2012). https://doi.org/10.1016/j.cej.2012.09.078
60. ZHU, Z., et al.: Absorption of Sb (III) from Aqueous Solution by the Porous Biomorph-Genetic Composition of $Fe_2O_3/Fe_3O_4/C$ Prepared with Bamboo Template, Industrial Safety and Environmental Protection, 06 (2016)
61. Zhang, S., et al.: Adsorption and desorption mechanisms of rare earth elements (REEs) by layered double hydroxide (LDH) modified with chelating agents. Appl. Sci. 9, 4805 (2019)

How to cite this article: Motallebi, R., et al.: Fabrication of superparamagnetic adsorbent based on layered double hydroxide as effective nanoadsorbent for removal of Sb (III) from water samples. IET Nanobiotechnol. 16(2), 33–48 (2022). https://doi.org/10.1049/nbt2.12074